Full-wave modeling in Wendelstein 7-X with Petra-M FEM

M. Verstraeten[1], S. Shiraiwa[2], J. Ongena[1], D. Castaño-Bardawil[1], D. Hartmann[3]
N. Bertelli[2], P. U. Lamalle[1], P. Dumortier[1], D. Van Eester[1], C. Slaby[3], F. Durodié[1]
F. Louche[1], G. C. Amanekwe[1], V. Maquet[1], B. Schweer[1] and the W7-X team[4]
[1]*Laboratory for Plasma Physics LPP-ERM/KMS, Brussels, Belgium*
[2]*Princeton Plasma Physics Laboratory, Princeton, NJ, USA*
[3]*Max-Planck-Institut für Plasmaphysik, Greifswald, Germany*
[4]*See the author list in paper O. Grulke et al., Nucl. Fusion 66 (2026) 116003*

Introduction

Interpreting ion cyclotron resonance frequency (ICRF) experiments in Wendelstein 7-X (W7-X) requires connecting the fields launched by the antenna to the conditions of a specific discharge. This is particularly demanding because the magnetic field, plasma boundary, antenna and close-fitting structures are three-dimensional, while the density and RF excitation must be assembled from several diagnostics and measurement systems. A useful full-wave model must preserve this device-specific complexity and maintain a traceable link to the experiment [1, 2].

Petra-M addresses this need by solving frequency-domain Maxwell equations in realistic 3-D geometry [3, 4]. This paper presents an experiment-informed workflow for full-wave ICRF modeling in W7-X with Petra-M, integrating antenna and vessel geometry, VMEC equilibria, reconstructed plasma densities and measured RF boundary conditions. The workflow is demonstrated for two W7-X discharges with different heating scenarios and strap phasing.

Experiment-informed Petra-M model

Geometry and electromagnetic problem. The vessel inner wall and plasma boundary were supplied as 751 cylindrical cross-sections and connected into surfaces. A simplified antenna CAD model permits tetrahedral meshing. The model distinguishes antenna-side vacuum (dark blue), cold-plasma core (purple) and lower-density edge regions (light blue) (Fig. 1). Metallic surfaces are perfect conductors; interfaces impose continuity of the tangential electromagnetic fields, while RF ports (red) and capacitor ports (orange) represent the feed and matching circuit.

For angular frequency ω, the complex electric field is obtained from the frequency-

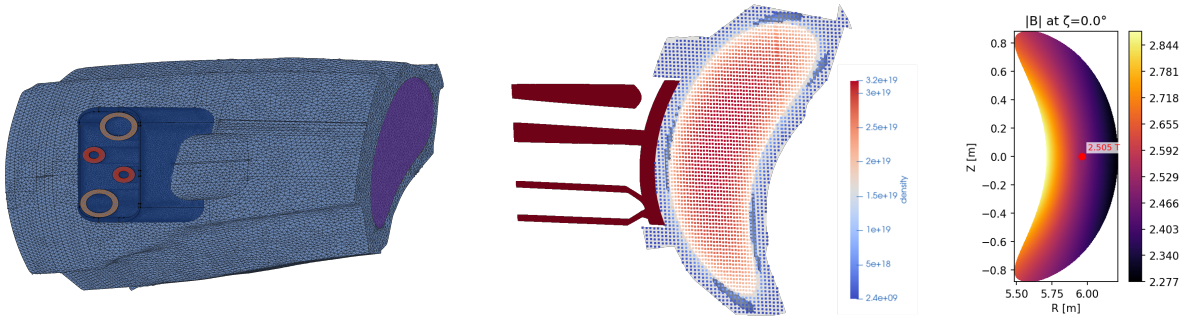

(a) computational mesh (b) reconstructed density (c) reconstructed $|B|$

Figure 1: Inputs to the W7-X Petra-M model: antenna/vessel mesh, combined plasma-density map, and VMEC-derived magnetic field.

domain curl–curl equation

$$\nabla \times \mu_r^{-1} \nabla \times \mathbf{E} - k_0^2 \boldsymbol{\varepsilon}_r(\mathbf{x}) \mathbf{E} = i\omega\mu_0 \mathbf{J}_{\mathrm{src}}, \qquad k_0 = \omega/c. \tag{1}$$

where the cold-plasma dielectric tensor depends on local density, composition and magnetic field. The present simulations use finite-element order 3, 1.5 million elements, and MUMPS. Collisional damping is included in the cold-plasma response through complex resonant denominators, with the damping inflated relative to physical collision rates to regularize the antenna-coupling problem and act as an absorption/radiative-boundary proxy. The resulting damping should therefore not be interpreted as a kinetic calculation of Landau or cyclotron heating.

Magnetic equilibrium and plasma profiles. VMEC represents nested 3-D flux surfaces by Fourier coefficients [5]. Geometry and field components are synthesized on angular grids, transformed to B_x, B_y, B_z, and interpolated onto a regular (R, Z, ϕ) grid. The field amplitude is rescaled to the experimental axis value, with the sign convention checked against the experimental coordinate convention. Extended surfaces cover the LCFS exterior; a separate island equilibrium is restored with five-fold symmetry. The magnetic configurations for shots 20241017.38 and 20250515.45 are KJM008+2520 and EIM000+2520.

The core fit is $n_e(\rho) = \Delta n_e(1-\rho^a)^b + n_{e1}$, where $\Delta n_e = n_{e0} - n_{e1}$ and $\rho = r_{\mathrm{eff}}/r_{\mathrm{LCFS}}$ is the normalized effective minor radius. Its parameters are obtained from Thomson-scattering data and assigned to VMEC surfaces. The SOL fit is $n_e(d) = n_f + (n_{e,\mathrm{LCFS}} - n_f)e^{-(d/\lambda)^p}$, where d is the distance from the LCFS along the profile-mapping direction. It is based on ICRH-side reflectometer data; n_f is the far-SOL density floor and the LCFS value is fixed by the core fit. A Gaussian fit to the Alkali-beam density bump supplies

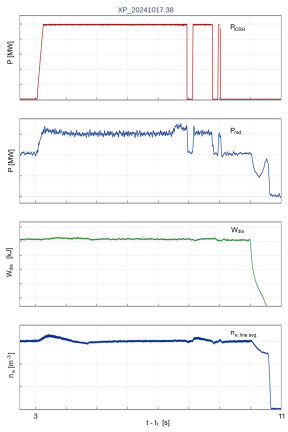

(a) shot 20241017.38

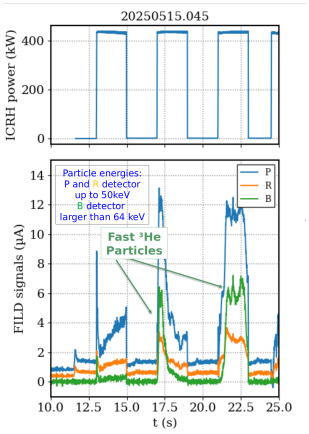

(b) shot 20250515.45

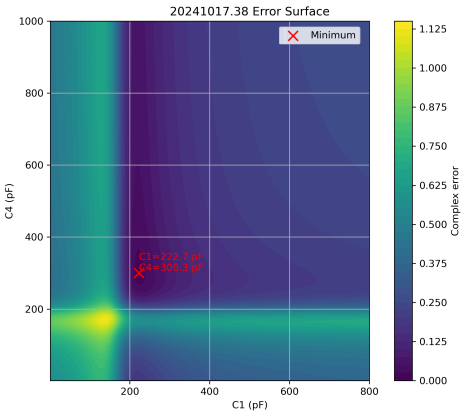

(c) preliminary capacitor fit

Figure 2: Experimental context and RF reconstruction: (a) minority-heating discharge traces; (b) modulated power and fast-ion-loss-detector signals for the three-ion discharge; (c) capacitor-fit error surface. The port-convention ambiguity remains unresolved.

the island contribution. For each discharge, the reconstruction workflow converts these fits and temperature profiles into Petra-M fields.

RF boundary conditions. Measured active reflection coefficients are translated to the antenna plane and compared with the Petra-M four-port S-matrix terminated by trial capacitances. Two fitted capacitors reduce it to an effective two-port system (Fig. 2c). A port-function interchange is presently needed to obtain a measurement-consistent minimum; its origin is unresolved, so this is a preliminary boundary reconstruction.

Preliminary application to two W7-X discharges

Two discharges were selected to exercise the workflow under distinct experimental conditions. Shot 20241017.38 (minority heating scenario) used a 6 s, 400 kW pulse at 25 MHz in hydrogen with about 2% ^{3}He and dipole strap phasing. Shot 20250515.45 (three-ion heating scenario) used modulated 400 kW ICRF in hydrogen with about 15% ^{4}He and at most 1% ^{3}He. Only one strap in monopole phasing was used for this experiment for technical reasons, although it is not the preferred phasing for heating. In the second case, fast-ion-loss-detector signals are synchronized with the ICRF modulation (Fig. 2b).

Figure 3 shows 3-D electric-field structure near the antenna and in the plasma.

The patterns differ, but a quantitative coupling comparison is still premature. The displayed field patterns alone do not establish damping, absorption or heating efficiency. The present result is therefore the demonstrated assembly and execution of an experiment-informed W7-X full-wave model.

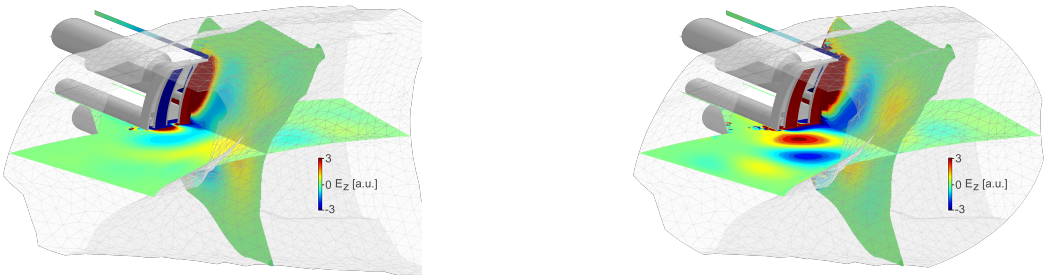

(a) minority heating

(b) three-ion heating scheme

Figure 3: Preliminary Petra-M full-wave ICRF simulation results for (a) shot 20241017.38 and (b) shot 20250515.45, using a cold-plasma model with core and edge density, normalized to unit port excitation.

Conclusions and outlook

A W7-X Petra-M workflow links realistic geometry, VMEC equilibria, diagnostic profiles and RF matching to a 3-D cold-plasma solve. It gives preliminary fields for minority- and three-ion-heating discharges. Next work will quantify loading, mode content and uncertainty sensitivity. Because the collisional damping is inflated mainly as a radiative boundary, anti-Hermitian dielectric power proxies are not physical heating predictions; quantitative core absorption and fast-ion predictions require kinetic follow-up with assumed $k_{\parallel}$ and cold-plasma $k_{\perp}$.

Acknowledgements. This work has been carried out within the framework of the EUROfusion Consortium, funded by the European Union via the Euratom Research and Training Programme (Grant Agreement No 101052200 — EUROfusion). Views and opinions expressed are however those of the author(s) only and do not necessarily reflect those of the European Union or the European Commission. Neither the European Union nor the European Commission can be held responsible for them.

References

[1] J. Ongena et al. Recent developments in ion cyclotron resonance heating. *Physics of Plasmas*, 21:061514, 2014.

[2] R. C. Wolf et al. Major results from the first plasma campaign of the wendelstein 7-x stellarator. *Nuclear Fusion*, 57:102020, 2017.

[3] S. Shiraiwa et al. Rf wave simulation for cold edge plasmas using the finite element method. In *EPJ Web of Conferences*, volume 157, page 03048, 2017.

[4] R. Anderson et al. MFEM: A modular finite element methods library. *Computers & Mathematics with Applications*, 81:42–74, 2021.

[5] S. P. Hirshman and J. C. Whitson. Steepest-descent moment method for three-dimensional magnetohydrodynamic equilibria. *Physics of Fluids*, 26:3553–3568, 1983.